Applied Catalysis B: Environmental 136–137 (2013) 140–149

Contents lists available at SciVerse ScienceDirect

Applied Catalysis B: Environmental

journal homepage: www.elsevier.com/locate/apcatb

Oxygen-removal of dibenzofuran as a model compound in biomass derived bio-oil on nickel phosphide catalysts: Role of phosphorus

J.A. Cecilia[a], A. Infantes-Molina[b], E. Rodríguez-Castellón[a], A. Jiménez-López[a,*], S.T. Oyama[c,d]

[a] Departamento de Química Inorgánica, Cristalografía y Mineralogía (Unidad Asociada al ICP-CSIC), Facultad de Ciencias, Universidad de Málaga, Campus de Teatinos, 29071 Málaga, Spain
[b] Instituto de Catálisis y Petroleoquímica, CSIC, Cantoblanco, 28049 Madrid, Spain
[c] Department of Chemical Engineering, Virginia Polytechnic Institute and State University, Blacksburg, VA 24061, United States
[d] Department of Chemical Systems Engineering, The University of Tokyo, 7-3-1 Hongo, Bunkyo-ky, Tokyo 113-8656, Japan

ARTICLE INFO

Article history:
Received 7 November 2012
Received in revised form 23 January 2013
Accepted 28 January 2013
Available online 6 February 2013

Keywords:
Nickel phosphide (Ni_2P)
Dibenzofuran
Hydrodeoxygenation
Hydrotreatment

ABSTRACT

The hydrodeoxygenation (HDO) of dibenzofuran (DBF) was investigated over silica-supported nickel phosphide catalysts with low metallic loadings (2.5–10 wt.%) and with different initial P/Ni atomic ratios. The formation of the nickel phosphide phase as well as the textural, structural and acidic properties of the catalysts were evaluated by X-ray fluorescence (XRFS), H_2-temperature programmed reduction (H_2-TPR), X-ray diffraction (XRD), CO chemisorption at 35 °C, N_2 adsorption–desorption isotherms at −196 °C, NH_3-temperature programmed desorption (NH_3-TPD) and elemental analysis (CNHS). The effect of metallic loading, the initial P/Ni molar ratio as well as the feed O-concentration on the catalytic activity were studied. Characterization results reveal that smaller particle sizes are formed at lower metallic loadings and high P/Ni atomic ratios, and that the acidity increases linearly with the metallic loading pointing to nickel and phosphorous species as the acidic centers in reduced catalysts. Nickel phosphide catalysts display good activity and stability in the HDO of DBF, reaching high DBF conversion values at moderate temperatures (300 °C) and with high selectivity to bicyclohexane (BCH), the main deoxygenated product which was obtained by hydrogenation of both aromatic rings (HYD pathway). Catalyst deactivation due to coke was minimal due to the low strength of the acid sites, while the formation of water did not present an inhibiting effect even under high O-concentration. This behavior might occur because water interacts preferentially with the excess phosphorous present on the catalyst surface and thus nickel phosphide particles do not undergo oxidation.

1. Introduction

Depletion of petroleum reserves, new stringent environmental regulations and rapid growth of global energy consumption have led to an increasing interest and necessity to find alternatives to fossil fuels. As a kind of renewable energy resource, biomass has recently drawn considerable attention for the production of liquid fuels and chemicals [1]. A promising method for obtaining liquid fuels is biomass fast pyrolysis, but unfortunately the liquid products obtained contain high contents of oxygen containing compounds, about 15–40 wt.% in which water takes up to 30 wt.% [2,3]. The average composition of pyrolysis oils includes organic acids, aldehydes, ketones, furans, phenolic compounds, guaiacols, syringols and sugar based compounds [3]. The presence of these molecules with high oxygen content contributes to some deleterious properties of the biofuels, such as high viscosity, corrosiveness, poor heating value, immiscibility with hydrocarbon fuels, low chemical and thermal stability, as well as to undesirable formation of carbon deposits in parts of automotive engines upon combustion [4,5]. In order to improve the physical and chemical stability of these liquid precursors, the oxygen must be removed by a hydrodeoxygenation process (HDO) through cleavage of C–O bonds, producing water and/or carbon oxides as by-products. Oxygen elimination can be performed by decarboxylation (CDO) or fluid catalytic cracking (FCC) [6]. Oxygen removal can also be carried out with conventional hydrotreating processes which generally operate under high pressure (3–10 MPa) of hydrogen at moderate temperatures (300–500 °C) [7]. This is applied to petroleum fractions, as conventional crudes may contain up to 2 wt.% oxygen [7]. Hydrodeoxygenation (HDO), hydrodesulfurization (HDS), hydrodenitrogenation (HDN), hydrodemetallization (HDM) and the saturation of olefins/aromatics at high hydrogen pressure occur

* Corresponding author. Tel.: +34 595 213 18 76; fax: +34 595 213 20 00.
E-mail address: ajimenezl@uma.es (A. Jiménez-López).

0926-3373/$ – see front matter © 2013 Elsevier B.V. All rights reserved.
http://dx.doi.org/10.1016/j.apcatb.2013.01.047

during the hydrotreating process [8]. Common probe molecules to evaluate the catalyst performances in HDO reactions are derivative furan compounds [9–11] among which dibenzofuran is a very low reactivity compound [7] and therefore a good choice as a model molecule to test HDO capability.

The catalysts most frequently studied for HDO have been sulfided Mo/Al_2O_3 catalysts, promoted by elements of group 9–10 (Co, Ni) [12–14]. However these catalysts suffer a progressive deactivation during the HDO reaction due to the oxidation of the active phase [15], so this makes desirable the development of new efficient catalysts. For this reason, new compositions showing a good hydrogen transfer properties have been assayed in hydrotreating processes. Among these, noble metals [16–18], metal carbides [19,20], metal nitrides [21,22], metal borides [23] and transition metal phosphides [24–27] have been tested in HDO.

In the last decade, transition metal phosphides have attracted great attention as new hydroprocessing catalysts. A plethora of research articles has reported that transition metal phosphides show excellent properties in hydrotreating reactions due to the presence of phosphorous that provides an ensemble effect and high stability [28,29]. In this way, the effect of phosphorous content in the hydroprocessing performance of phosphides is becoming a key factor to consider. Oyama et al. have reported [29] that the HDS conversion goes through a maximum when a P/Ni molar ratio of 3 was employed. In recent years, several studies have revealed that supported transition metal phosphides such as Ni_2P/SiO_2 [25,29], MoP/SiO_2 [25] and Ru_2P/SiO_2 [27] have shown high conversion in the HDO of phenol, furan, benzofuran, guaiacol and anisole.

In this work the formation, activity and catalytic stability of nickel phosphide catalysts in the HDO of dibenzofuran (DBF) is investigated. These catalysts have been synthesized according to a method previously described [30] that uses a precursor salt containing an excess of phosphorous. In the present study the P/Ni initial ratio, the metallic loading as well as the O-concentration in the feed are studied focusing on the role of phosphorous on the catalytic performance of these systems.

2. Experimental

2.1. Materials

The support used in this study was a commercial silica (Cab-o-Sil M-5, Riedel-de Haen, Sigma–Aldrich). The reagents used to prepare the catalyst precursors were phosphorous acid (H_2PO_3H, Aldrich 99%), and nickel(II) hydroxide ($Ni(OH)_2$, Aldrich 99%). The chemical products utilized in the reactivity study were dibenzofuran (Aldrich 98%) dissolved in cis-, trans-decahydronaphthalene (Sigma–Aldrich 98%). The gases employed were He (Air Liquide 99.99%), H_2 (Air Liquide 99.999%), N_2 (Air Liquide 99.9999%), NH_3 (Air Liquide 99.9%) and CO (Air Liquide 99.9%).

2.2. Preparation of catalysts

Phosphorus and nickel were introduced by the incipient wetness impregnation method using a solution of nickel(II) dihydrogenophosphite ($Ni(HPO_3H)_2$) as precursor, prepared from stoichiometric amounts of nickel(II) hydroxide ($Ni(OH)_2$) and phosphorous acid (H_2PO_3H). The support employed was a commercial silica Cab-o-Sil due to its purity and inherent inertness as a support [31,32]. After the nickel aqueous salt solution was added to the pelletized support (0.85–1.00 mm), it was air dried, and then treated by temperature programmed reduction (H_2-TPR) to convert the precursor phosphite into phosphide. For this purpose, 80 mg of sample were placed in a tubular reactor with a heating rate of 3 °C min^{-1} and a hydrogen flow rate of 100 mL min^{-1}. These reduction conditions have been optimized in previous works [30,32]. The concentration of the precursor solutions were adjusted to the desired metal loading. Four catalysts were prepared with a nickel loading ranging from 2.5 to 10 wt.% of Ni. The prepared catalysts will be referred to as Ni_2P-*x*, where *x* represents the percentage in weight of nickel present in the sample.

Furthermore another series of nickel phosphide catalysts were also prepared by H_2-TPR, keeping constant the nickel content (5 wt.% Ni) and varying the initial phosphorous content. The samples prepared had initial P/Ni molar ratios of 1, 2 and 3, respectively. Thus,Ni_2P-5-P/Ni = 2 is prepared by adding stoichiometric amounts of $Ni(OH)_2$ and H_2PO_3H to the incipient volume to form the precursor salt $Ni(HPO_3H)_2$ containing 5 wt.% of Ni. Similarly, Ni_2P-5-P/Ni = 1 is synthesized by mixing $Ni(HPO_3H)_2 + Ni(OH)_2$ (5 wt.% Ni and P/Ni atomic ratio = 1). Finally, Ni_2P-5-P/Ni = 3 is prepared by mixing $Ni(HPO_3H)_2 + H_2PO_3H$ (5 wt.% Ni and P/Ni atomic ratio = 3).These catalysts will be denoted as Ni_2P-5-P/Ni = *y*, *y* being the initial P/Ni ratio present on each sample.

2.3. Characterization of catalysts

Elemental bulk composition of the catalysts in terms of Ni and P loading was determined by X-ray fluorescence spectrometry (XRFS) using a Horiba XGT-500 spectrometer with a probe diameter of 1.2 mm. The X-ray tube was set at 50 kV with an acquisition time of 500 s and a current intensity between: 0.26 and 0.32 mA.

The temperature programmed reduction of the precursor phosphite to nickel phosphide was carried out by placing 80 mg of precursor in a tubular reactor, with heating at a linear temperature ramp (3 °C min^{-1}) in flowing hydrogen (100 mL min^{-1}) from 100 to 800 °C. The evolved gases were sampled in a quadrupole mass spectrometer Balzer GSB 300 02 equipped with a Faraday detector (0–200 uma), and the masses 2 (H_2), 18 (H_2O), 31 (P), 34 (PH_3) and 124 (P_4) were monitored during the experiment. The signals and temperature were recorded in real time by an online computer.

Powder diffraction patterns were collected on an X'Pert Pro MPD automated diffractometer equipped with a Ge(1 1 1) primary monochromator (strictly monochromatic Cu-Ka radiation) and an X'Celerator detector.

CO chemisorption analyses were performed under static volumetric conditions in a Micromeritics ASAP 2020 apparatus. Samples were reduced ex situ and transferred in an inert atmosphere. Prior to measurement, samples were re-reduced in situ in H_2 at 300 °C and evacuated at 25 °C for 10 h. The chemisorption isotherm was obtained by measuring the amount of CO adsorbed between 10 and 600 mmHg at 35 °C. After completing the initial analysis, the reversibly adsorbed gas was evacuated and the analysis repeated to determine only the chemisorbed amounts.

The textural parameters (S_{BET}, V_P and d_P) were evaluated from nitrogen adsorption–desorption isotherms at −196 °C as determined by an automatic ASAP 2020 system from Micromeritics. Prior to the measurements, samples were outgassed at 200 °C and 10^{-4} mbar overnight. Surface areas were determined by using the Brunauer–Emmett–Teller (BET) equation and a nitrogen molecule cross section of 16.2 $Å^2$. The pore size distribution was calculated by applying the Barret–Joyner–Halenda (BJH) method to the desorption branch of the N_2 isotherm. The total pore volume was calculated from the adsorption isotherm at $P/P_0 = 0.996$.

The temperature-programmed desorption of ammonia (NH_3-TPD) was carried out to evaluate the total surface acidity of the catalysts. A quantity of 80 mg of catalyst precursor was reduced at atmospheric pressure by flowing hydrogen (100 mL min^{-1}) with a heating rate of 3 °C min^{-1} from room temperature to the reduction temperature established in the H_2-TPR. After flushing with helium and adsorption of ammonia at 100 °C, NH_3-TPD using a helium flow was performed by raising the temperature from 100 to 550 °C at a

heating rate of 10 °C min^{-1} followed by an isothermal period at 550 °C for 15 min. The evolved ammonia was analyzed by online gas chromatography (Shimadzu GC-14A) equipped with a TCD. In order to quantify the amount of desorbed ammonia, the equipment was previously calibrated by measuring the corresponding signals of the thermal decomposition of known amounts of hexaamminenickel(II) chloride $[Ni(NH_3)_6]Cl_2$.

Elemental chemical analysis was performed for spent catalysts with a LECO CHNS 932 analyzer to determine the carbon content present after the catalytic test through the combustion of the samples at 1100 °C to form CO_2.

X-ray photoelectron spectra were collected without exposure to the atmosphere using a physical electronics PHI 5700 spectrometer with non monochromatic Al Kα radiation (300 W, 15 kV and 1486.6 eV) with a multi-channel detector. Spectra of pelletized samples were recorded in the constant pass energy mode at 29.35 eV, using a 720 μm diameter analysis area. Charge referencing was measured against adventitious carbon (C 1*s* at 284.8 eV). A PHI ACCESS ESCA-V6.0 F software package was used for acquisition and data analysis. A Shirley-type background was subtracted from the signals. Recorded spectra were fitted using Gaussian–Lorentzian curves in order to determine the binding energies of the different element core levels more accurately. Reduced and spent catalysts were stored in sealed vials with an inert solvent. The sample preparation was done in a dry box under a N_2 flow, where the solvent was evaporated prior to its introduction into the analysis chamber, and directly analyzed without previous treatment.

2.4. Catalytic test

For the catalytic test, the hydrodeoxygenation of DBF was chosen, which was performed in a high-pressure fixed-bed continuous-flow stainless steel catalytic reactor (9.1 mm in diameter, and 230 mm in length), operated in a down-flow mode. The reaction temperature was measured with an internal thermocouple in direct contact with the catalyst bed. The organic feed consisted of solutions of DBF at levels from 10,000 ppm to 40,000 ppm in a solvent of cis–trans-decahydronaphthalene that was supplied by means of a Gilson 307SC piston pump (model 10SC). For the activity tests, 0.5 g of catalyst were used (particle size 0.85–1.00 mm) which were diluted with quartz sand to 3 cm^3. Prior to the activity test, the catalysts were reduced in situ at atmospheric pressure with a H_2 flow of 100 mL min^{-1} by heating from r.t. to the reduction temperature (550 °C) with a heating rate of 3 °C min^{-1}. Catalytic activities were measured at different temperatures (200–300 °C), under 3.0 MPa of H_2, at a flow rate of 100 mL min^{-1}. The catalysts were previously stabilized for 12 h. Temperature was varied as follows: 300 °C → 250 °C → 200 °C → 225 °C → 275 °C → 300 °C, with the reaction held at each temperature for 4 h. The stabilities of the catalysts were determined at a constant temperature (300 °C) for 12 h. The evolution of the reaction was monitored by collecting liquid samples after 60 min at the desired reaction temperature. These liquid samples were kept in sealed vials and subsequently analyzed by gas chromatography (Shimadzu GC-14B, equipped with a flame ionization detector and a capillary column, TBR-14, coupled to an automatic Shimadzu AOC-20i injector). For these catalysts, the main products of the reaction were biphenyl (BP), cyclohexylbenzene (CHB), bicyclohexane (BCH), benzene (B) and cyclohexane (CH). For this reason, the total conversion was calculated from the ratio of converted dibenzofuran/initial dibenzofuran. The selectivity to the different reaction products was calculated considering BP, CHB, B and CH as the only products obtained, since only slight traces of some unknown compounds were noticeable in a few cases.

The turnover frequency was calculated from the formula:

$$\mathrm{TOF} = -\frac{\ln(1-X)}{(W/F)\times M} \quad (1)$$

where F is the molar rate of reactant (mol min^{-1}), W is the catalyst weight (g), X is the conversion and M is the mole of sites loaded (mol g^{-1}). This formula was used because the conversions were close to 100% so were far from differential conditions, and an integral analysis was needed. This equation, in which $-\ln(1-X)$ substitutes for X assumes a pseudo first-order reaction which may be justified by the large excess of hydrogen.

3. Results and discussion

3.1. Elemental analysis

Table 1 reports the nickel and phosphorus contents for reduced catalysts as determined by X-ray fluorescence spectroscopy. Catalysts prepared with different metallic loadings present in all cases a Ni/P ratio close to 2, the expected value if the Ni_2P phase is formed. By varying the initial P/Ni atomic ratio, catalysts with lower or higher amounts of phosphorus can be obtained.

3.2. Temperature-programmed reduction of precursor catalysts

The synthesis of the nickel phosphide catalysts was carried out by H_2-TPR for all catalysts. The profiles of similar catalysts have been described in a previous study [32]. The curves corresponding to the evolved H_2O and PH_3 for the precursors with different P/Ni ratios are shown in Fig. 1A and B. The water formation curves (Fig. 1A) show an initial small peak (460 °C) followed by a larger peak at a moderate temperature (600 °C) for all catalysts. The findings are in agreement with previous studies [29,33]. Moreover, all the samples present a slight water signal at low temperatures (200–300 °C) ascribed previously to the hygroscopic character of the precursor salt [32]. These results on precursors presenting different P/Ni ratio clearly show that by increasing phosphorous content the reduction temperature shifts to higher values. Fig. 1A

Table 1
Chemical analysis[a], CO uptakes[b], dispersion[b] and particle size of reduced Ni_2P/SiO_2 based catalysts.

	Ni/P[a]	CO uptake (μmol g^{-1})[b]	Dispersion (%)[b]	Particle size (nm)[c]
Ni_2P-2.5	1.7	26	6.3	14
Ni_2P-5	2.0	36	4.2	21
Ni_2P-7.5	2.0	45	3.5	25
Ni_2P-10	2.0	49	2.9	31
Ni_2P-5-P/Ni = 1	2.7	31	3.6	25
Ni_2P-5-P/Ni = 2	2.0	36	4.2	21
Ni_2P-5-P/Ni = 3	1.7	73	8.6	10

[a] Bulk molar ratios determined by XRFS.
[b] As determined from CO chemisorption measurements at 35 °C.
[c] Calculated from the equation $d \approx 0.9/D$ according to Ref. [26].

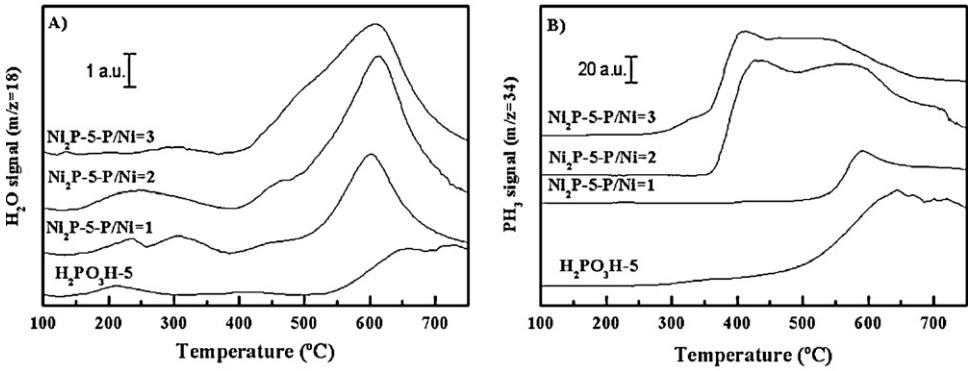

Fig. 1. H_2-TPR curves of Ni_2P supported catalysts: (A) water profiles of Ni_2P-5-P/Ni = *y* precursors and (B) phosphine profiles of Ni_2P-5-P/Ni = *y* precursors. Reduction conditions: 100 ml min^{-1} H_2 and heating rate 3 °C min^{-1}.

also shows that besides the slight shift to higher temperatures, an increase in water loss is also observed due to the higher amount of HPO_3H^- ions present. Moreover, the profile of the sample with the lowest P/Ni molar ratio (P/Ni = 1), presenting an excess of Ni in the form of $Ni(OH)_2$, shows two reduction peaks at lower temperatures. Bando et al. [34] established by QXAFS that the decomposition of $Ni(OH)_2$ takes place at about 150 °C giving rise to atomically dispersed Ni^{2+} species which are stabilized by interaction with the support, which later are reduced to form the Ni_2P phase. On the other hand, Fig. 1B shows the corresponding curves of PH_3 formation. The evolution of the curves follows the same trend as those of water formation, i.e., an initial peak at low temperatures (400 °C) and a second one at ca. 600 °C. The PH_3 formation increases with the P content, as expected.

The chosen reduction temperature was 550 °C taking into account that the maxima in water profiles (Fig. 1) are close to 600 °C and that shifts in reduction to higher temperature occur during temperature programming. All catalysts were maintained at this temperature for 2 h to ensure complete phosphidation of the samples.

3.3. X-ray diffractograms

X-ray diffraction (XRD) patterns were used to identify the crystalline phases formed after reduction (Fig. 2). All catalysts show a broad diffraction line located at $2\theta = 23–25°$, typical of amorphous silica and diffraction lines at $2\theta = 40.7°$, 44.6°, 47.4°, 54.2° and 55.0° (PDF 01-089-4864) corresponding to the Ni_2P phase. The diffraction profiles of catalysts with low nickel loading show less well-defined and broadened diffraction features. As previously observed, silica favors the formation of nickel phosphide with a small particle size and high dispersion [32,35]. By increasing nickel and phosphorous loading (Fig. 2A) the diffraction lines become more intense due to the formation of increasing amounts of Ni_2P phase, which is also more crystalline (vide infra). However X-ray diffractograms of catalysts with different P/Ni ratios (Fig. 2B) present different characteristics. Thus, the sample with the lowest P content exhibits, besides the diffraction lines due to the Ni_2P phase, others lines at $2\theta = 39.8°$, 41.3°, 41.7°, 44.4°, 47.0° and 48.9° due to the presence of $Ni_{12}P_5$ (PDF 01-074-1381). The formation of a nickel rich phosphide is expected due to the lower P/Ni molar ratio in this sample, however the Ni_2P phase is always observed. Rodriguez et al. [36] pointed that $Ni_{12}P_5$ is an intermediate in the formation of Ni_2P, and its observation reflects the low content of phosphorus. For the higher P/Ni ratio of 3, the lack of formation of phosphorus-rich compounds such as NiP_2 indicates that Ni_2P is particularly favored. The unutilized phosphorus is converted to gaseous PH_3 and partly deposited on the support as phosphate, as can be deduced from Fig. 1B.

3.4. CO chemisorption measurements

The CO chemisorption capacities for the reduced catalysts provide the number of surface nickel atoms (*n*CO) and an estimate of the active sites. Table 1 reports the CO uptakes at room temperature for nickel phosphide catalysts and the dispersion (D) of metal sites estimated from the CO uptakes. The uptakes range from 26 to 49 μmol g^{-1} and rise with the metallic content, which indicates that the number of active sites also increases. However the calculated dispersion decreases with the metallic content, and this is understandable as larger crystallite sizes are formed with increasing metallic loading. On the other hand, for catalysts prepared

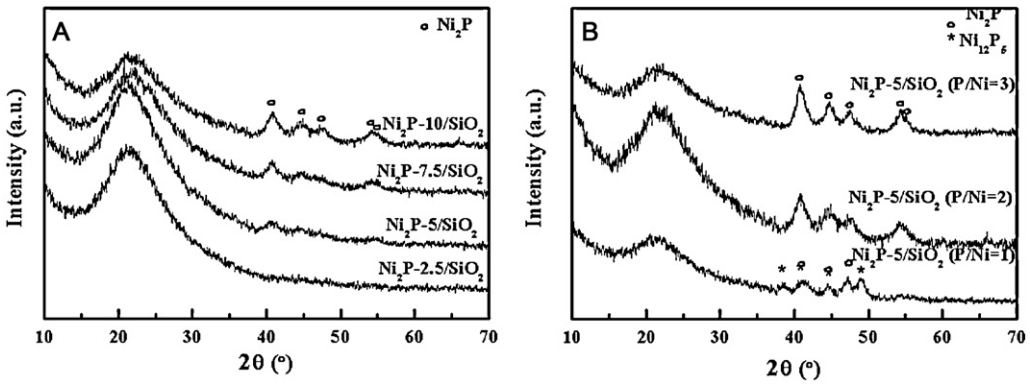

Fig. 2. X-ray diffractograms of fresh catalysts. (A) Influence of nickel loading and (B) Influence of P/Ni initial molar ratio. Reduction conditions: 100 ml min^{-1} H_2 and heating rate 3 °C min^{-1}.

with different P/Ni initial molar ratios, the metal site concentration increases with the phosphorous content in the samples accompanied with an increase in the dispersion. The particle size (d) was then calculated using the equation $d \approx 0.9/D$ [26]. The obtained values are also included in Table 1. The general trend observed is the formation of smaller nickel phosphide particles when using a low metallic loading or a phosphorous excess, i.e. Ni_2P-2.5 and Ni_2P-P/Ni = 3. These results are in agreement with the previously presented XRD results, which pointed to a better dispersion of the active phase for the catalyst with the lowest metallic loading, and therefore presenting a greater number of active sites. Extra phosphorus seems to favor the dispersion of the metallic phase. In this sense, Oyama et al. [29] have indicated that a higher proportion of phosphorous species in Ni_2P/SiO_2 catalysts increases the dispersion of nickel on a silica support.

3.5. Textural parameters

Table 2 summarizes the textural properties of the supported nickel phosphide catalysts. The catalysts suffer a progressive loss of surface area when the precursor loading or the P/Ni initial ratio increases. This is because of a slight blockage of pores due to the presence of nickel phosphide particles on the silica support which hampers access of gas molecules. Such pore blockage has been reported before for high P/Ni molar ratios and was ascribed to the deposition of the phosphorous excess on the pore surfaces [29,37]. A phosphorous excess is necessary in this case to form the $Ni(HPO_3H)_2$ precursor salt, P/Ni = 2, when the theoretical value to form Ni_2P phase is 0.5. Thus, by increasing the P/Ni molar ratio, the surface area decreases. Nonetheless, a phosphorous excess is reported to be necessary for the formation of Ni_2P and to maintain Ni_2P particles fully phosphided during reaction [38].

3.6. Acidic properties

The acidic properties of the catalysts were measured by temperature-programmed desorption of ammonia (NH_3-TPD) between 100 and 550 °C. Table 2 compiles the amount of desorbed NH_3 (mmol of NH_3 g^{-1}) for the support and reduced catalysts. From the acidity data it can be seen that the concentration of acid sites as well as the acid site density increase with both the metallic loading and the P/Ni initial molar ratios, which implies that the presence of phosphorus and nickel are responsible for the increase. The total acidity is due to both the presence of Brönsted and Lewis acid sites. Abu and Smith [39] reported that the source of Brönsted sites is phosphate species, remaining as a consequence of their incomplete reduction. The presence of Lewis sites has been observed by several researchers [25,40], who have suggested that Lewis acidity on nickel phosphide may be ascribed to nickel species bearing a small positive charge due to electron transfer from nickel to phosphorus. The acidity is increased much more by raising the metallic loading than by increasing the amount of phosphorous, as can be seen from Table 2. Therefore, it is not only the phosphorus excess that contributes to ammonia adsorption but also the presence of nickel. These centers have been considered as the active sites for hydrogenolysis and hydrogenation processes in the HDO reaction [25].

The strength of the acid sites can be determined by the temperature at which the adsorbed NH_3 starts to desorb. Based on the desorption temperature, the acid sites can be classified as weak ($T < 250$ °C) and strong ($T > 250$ °C). As seen in Table 2, all Ni_2P catalysts showed weak and strong acid sites.

3.7. Catalytic results

The prepared catalysts have been tested in the HDO of dibenzofuran. The reaction routes that may occur during HDO of DBF are shown in Scheme 1. The formation of the products and intermediates has been previously discussed in the literature [41,42]. Briefly, there is a hydrogenation (HYD, pathway 1), in which oxygen removal is preceded by hydrogenation of benzene rings; a direct deoxygenation (DDO, pathway 3), in which oxygen removal occurs by direct cleavage of bonds linking oxygen to aromatic carbons; and an intermediate pathway (pathway 2) in which oxygen removal is preceded by hydrogenation of only one benzene ring.

First, the activity related to the loading of nickel phosphide on the catalyst was studied. Fig. 3 depicts the HDO conversion as a function of the reaction temperature. All catalysts present an increasing conversion with temperature. At low temperatures (200 °C), all the catalysts show low conversion values, ranging from 17 to 29%. The conversion depends on the nickel phosphide loading, increasing from 2.5 up to 7.5 wt.%, but incrementing the loading further leads to lower conversion. This behavior could probably be ascribed to the low catalyst charge for the Ni_2P-2.5 catalyst and the lower active phase dispersion for the Ni_2P-10 sample. By increasing the temperature, the conversion rises for all the catalysts with values higher than 90%, except for the Ni_2P-2.5 sample which shows a lower value (74%).

The activity per active site (TOF), calculated from CO chemisorption, is higher (at 200 °C) for the catalysts with an intermediate loading, 5 and 7.5 wt.%. At 300 °C, TOF number increases for all the samples, with the Ni_2P-7.5 and Ni_2P-10 catalysts showing the highest activity.

With regards to HDO selectivity, the main oxygen-free compounds products detected were: bicyclohexane (BCH), cyclohexylbenzene (CHB), biphenyl (BP) and single ring products

Table 2
Textural and acidic properties of the pure support and reduced Ni_2P/SiO_2 catalysts.

Samples	S_{BET} (m^2 g^{-1})[a]	V_{ads} (cm^3 g^{-1})[a]	Amount of acid sites (mmol NH_3 g_{cat}^{-1})[b]		Acid sites density (μmol NH_3 m^{-2})[b]
			Weak $T < 250$ °C	Strong $T > 250$ °C	
SiO_2	204	0.699			
Ni_2P-2.5	179	0.574	1.8	1.3	17.3
Ni_2P-5	162	0.541	2.2	1.8	24.7
Ni_2P-7.5	148	0.514	3.5	1.9	36.5
Ni_2P-10	132	0.597	3.3	3.0	47.7
Ni_2P-5-P/Ni = 1	178	0.595	1.7	1.5	18.0
Ni_2P-5-P/Ni = 2	162	0.541	2.2	1.8	24.7
Ni_2P-5-P/Ni = 3	145	0.586	2.2	2.1	29.7

[a] As determined from N_2 adsorption–desorption isotherms at −196 °C.
[b] As determined from NH_3-TPD measurements.

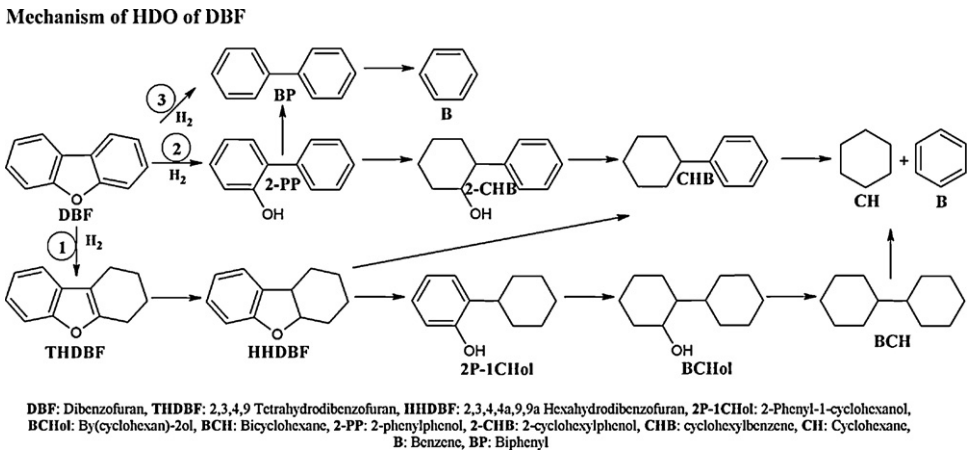

DBF: Dibenzofuran, THDBF: 2,3,4,9 Tetrahydrodibenzofuran, HHDBF: 2,3,4,4a,9,9a Hexahydrodibenzofuran, 2P-1CHol: 2-Phenyl-1-cyclohexanol, BCHol: By(cyclohexan)-2ol, BCH: Bicyclohexane, 2-PP: 2-phenylphenol, 2-CHB: 2-cyclohexylphenol, CHB: cyclohexylbenzene, CH: Cyclohexane, B: Benzene, BP: Biphenyl

Scheme 1. Reaction pathways for HDO of DBF [7].

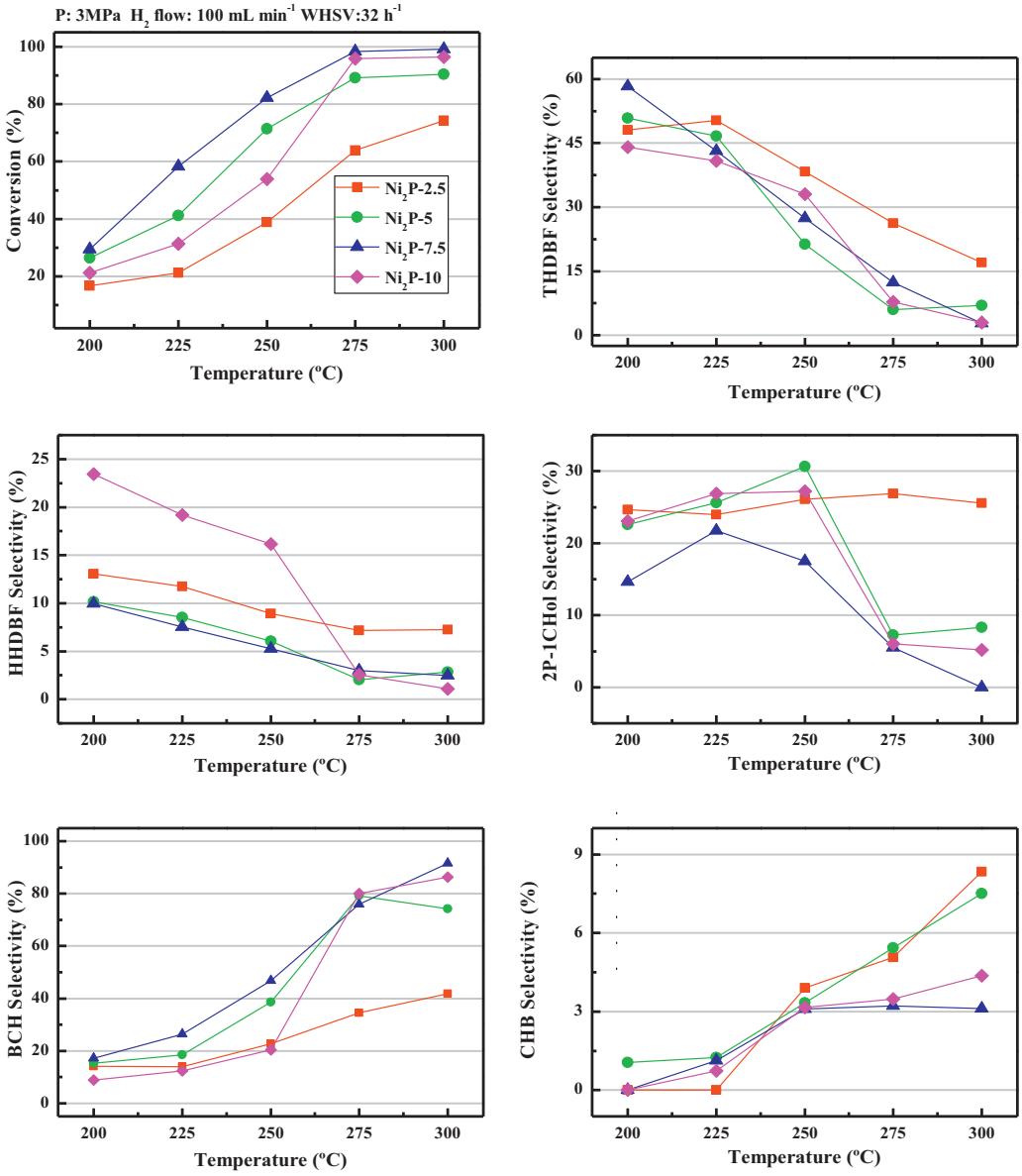

Fig. 3. Evolution of conversion and selectivity as a function of reaction temperature for Ni_2P-x/SiO_2 catalysts with different Ni_2P loadings. Feed: 20,000 ppm of DBF.

as benzene (B) and cyclohexane (CH) but in minor quantities. The oxygen-containing intermediates observed were tetrahydrodibenzofuran (THDBF), hexahydrodibenzofuran (HHDBF) and 2-phenyl-1-cyclohexanol (2P-1CHol). Fig. 3 shows how the selectivity to different reaction products changes with reaction temperature. At low temperatures (200 °C), O-containing intermediates (THDBT, HHDBT and 2P-1CHol) are formed in the highest proportions, above 80% in all cases. As the reaction temperature increases, so too does the formation of BCH. The selectivity to BCH at 300 °C follows the order: Ni_2P-7.5 (92%) > Ni_2P-10 (86%) > Ni_2P-5 (74%) ≫ Ni_2P-2.5 (42%). In general, all the catalysts follow the same selectivity pattern. The catalyst with the lowest metallic content is the least active at all studied temperatures and presented the highest amount of O-containing intermediates.

Furimsky et al. [7] suggested that the HDO reaction of DBF could follow several pathways depending on the reaction temperature (Scheme 1). At low temperatures, the HDO of dibenzofuran follows route (1) whereby pre-hydrogenation of the aromatic rings takes place first, followed by rapid C–O bond rupture leading to a saturated cyclic product such as bicyclohexane (BCH). At moderate temperatures HDO follows route (2) whereby hydrogenation of one aromatic ring occurs first, followed by deoxygenation by C–O bond cleavage or OH elimination, forming cyclohexylbenzene (CHB) as the main reaction product. Finally, at high temperatures HDO follows the direct deoxygenation route (3), where the main product biphenyl (BP) is formed without phenolic intermediates. This scheme is reasonable because it involves aromatic species at high temperature which are expected due to the exothermic character of hydrogenation reactions, and also because the cleavage of oxygen-sp^2 carbon bonds is more difficult than oxygen-sp^3 carbon bonds so it is possible at higher temperatures. A similar reaction mechanism was established by Krishnamurthy et al. [41], who suggested that the cleavage of the C–O bond takes place at low and moderates temperatures to first give rise to phenylphenol and cyclohexylphenol, respectively. Subsequently, deoxygenated compounds are formed in secondary reactions involving the hydrogenated intermediates. In a recent study, Romero et al. [9] studied the intermediates and products of HDO of benzofuran over $NiMoP/Al_2O_3$ catalysts and suggested the existence of three routes: a hydrogenation pathway (HYD) (1), a pathway involving the acid properties of the catalysts (ACI) (2) and a direct deoxygenation pathway (DDO) (3). Previous researchers have established that all the phenolic intermediates are more reactive [43,44] than dibenzofuran and that it is why no phenolic intermediates are observed as byproducts. Also, Bunch et al. [10] have reported that the HDO reaction of benzofuran takes place by multiple steps of hydrogenation and hydrogenolysis of the phenolic intermediates which occur by β hydrogen elimination (E_2) or nucleophilic substitution (S_{N^2}).

The experimental data presented here reveal the presence of O-containing intermediates, indicating that under the experimental conditions employed they are not very reactive. Fig. 4A depicts the evolution of the selectivity as a function of the conversion attained for Ni_2P-5 catalyst. From this figure it can be seen that at low temperature the main products detected are O-containing intermediates, mainly tetrahydrodibenzofuran (THDBF, 51%), 2-phenyl-1-hexanol (2P-1CHol, 23%) and hexahydrodibenzofuran (HHDBF, 10%). The selectivity to HHDBF was always lower than that observed to 2P-1CHol and this suggests that the transformation of HHDBF to 2P-1CHol was favored, probably due to the higher reactivity of this intermediate. From Fig. 4A it is observed that THDBF and HHDBF selectivity decreases with conversion, while that of 2P-1CHol slightly increases up to maximum at a conversion of about 70% and then decreases as the formation of BCH is more favored.

These data indicate that Ni_2P based catalysts undergo the HDO of DBF through pathway 1 under the experimental conditions employed: i.e., DBF → THDBF → HHDBF → 2P-1CHol → BCH and represented in Scheme 2, this transformation is favored by increasing the temperature from 200 °C to 300 °C. Thus, at 300 °C, a greater proportion of O-free compounds, mainly BCH, is present. Fig. 4B shows the yields to O-free compounds (BCH + CHB) for these catalysts at 300 °C. Except for the catalyst with the lowest metallic loading (2.5 wt.%), all of the samples show high yields (>75%), indicating that the catalysts are highly effective in O-removal reactions even at low metallic loadings such as 5 wt.%.

The bi-functional catalysis for hydrodeoxygenation requires a metallic function for hydrogenation and an acid function for hydrogenolysis, dehydration, and isomerization. The balance between these functions determines the observed catalytic activity [45]. The high hydrogenation ability in phosphides has been assigned to their displaying-metal-like properties, which contribute to a strong hydrogenating capability similar to transition metals [40]. Some authors have related the metal-like properties to $Ni^{\delta+}$ sites bearing a small positive charge that not only act as Lewis acid sites but also as metal sites for hydrogenolysis and hydrogenation [25]. Romero et al. [9] have reported that over sulfided $NiMoP/Al_2O_3$ catalysts the deoxygenation takes place by a direct

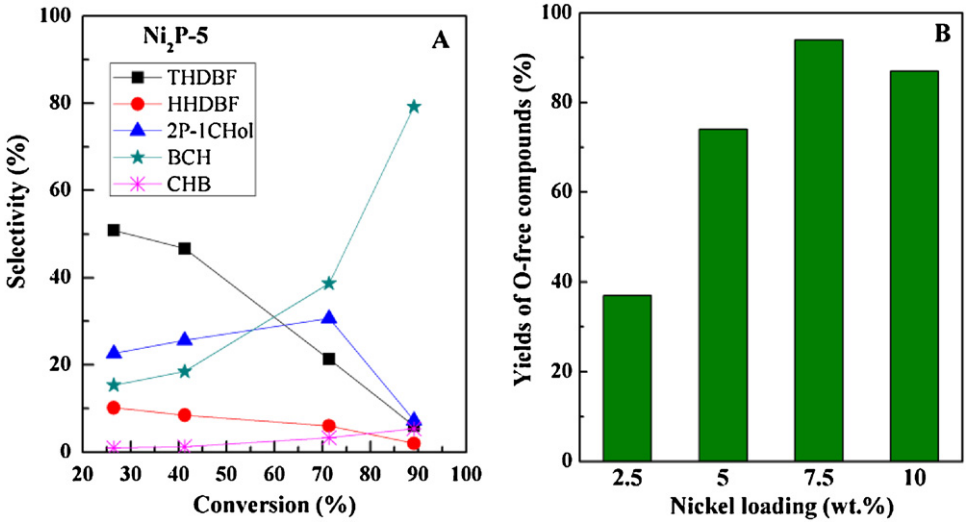

Fig. 4. Evolution of selectivity as a function of conversion for Ni_2P-5 catalyst (A) and Yields of O-free compounds (BCH + CHB) versus catalysts composition at 300 °C (B). Experimental conditions: P = 3.0 MPa; WHSV = 32 h^{-1}; Feed: 20,000 ppm of DBF.

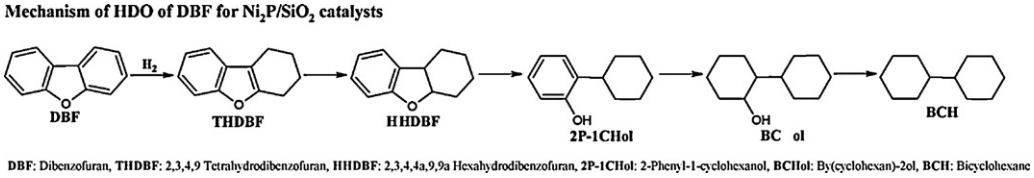

Scheme 2. Reaction pathways for HDO of DBF over Ni_2P/SiO_2 catalysts.

hydrogenolysis reaction instead of a dehydration reaction due to the presence of unreduced phosphorous that increases the Brönsted acidity of the catalyst. Nonetheless Li et al. [22] suggest that PO-H groups, which act as Brönsted sites and provide active hydrogen species, had less activity for the hydrogenation, hydrogenolysis and dehydration reaction compared to the metal $Ni^{\delta+}$. The hydrogenation capability observed for Ni_2P catalyst could be ascribed to both the presence of $Ni^{\delta+}$ sites acting as metal like sites and the presence of unreduced phosphorus with Brönsted acidity that provides active hydrogen species. Thus Ni_2P acts as a bi-functional catalyst displaying acidic and metallic properties with strong hydrogenating capabilities similar to noble metal catalysts on acidic supports [24]. The results exhibited by these catalysts are in agreement with previous studies, where transition metal phosphide based catalysts displayed high selectivity toward hydrogenated products [25,46]. In this sense, Ueckert et al. [47] have proposed that nickel sites with a high electron density favors the formation of π back bonds between aromatic rings and metal sites, promoting the hydrogenation of the rings.

The selectivity pattern presented by Ni_2P catalysts in the HDO of DBF reaction is different to that previously observed in the HDS of DBT. Due to the similarity of both molecules and the same type of catalyst, it is expected that the heteroatom removal pathway would be the same. In contrast, while the HDS of DBT over nickel phosphide catalyst followed the direct desulfurization route (DDS) [30,32], the HDO of DBF followed the hydrogenation route. The different selectivity found for HDO of DBF and HDS of DBT could be based on the nature of heteroatoms in these molecules. Thus, DBT with a sulfur atom having empty d orbitals interacts with metallic sites with π back bonding from metal to sulfur. In contrast, the oxygen atom in DBF lacks d orbitals and cannot interact with metallic centers trough this type of bond, thus this molecule interacts through the π orbital of the aromatic rings leading to their hydrogenation.

The catalyst stability with time on stream was evaluated for 12 h at 300 °C feeding different DBF quantities (10,000, 20,000 and 40,000 ppm). The catalyst tested was Ni_2P-5, an intermediate Ni_2P loading, which presented high conversion and TOF (Table 3). A high stability is observed for 10,000 and 20,000 ppm of DBF (Fig. 5).

Table 3
HDO rates and TOF values for Ni_2P catalysts.

Samples	Conversion (%)		TOF (h^{-1})	
	200 °C	300 °C	200 °C	300 °C
Ni_2P-2.5[a]	17	74	0.4	3
Ni_2P-5[a]	26	90	0.5	4
Ni_2P-7.5[a]	29	99	0.5	7
Ni_2P-10[a]	22	96	0.3	4
Ni_2P-5-10,000	99		5	
Ni_2P-5-20,000	99		9	
Ni_2P-5-40,000	98		14	
Ni_2P-5-P/Ni = 1[a]	88		4	
Ni_2P-5-P/Ni = 2[a]	99		9	
Ni_2P-5-P/Ni = 3[a]	97		2	

Experimental conditions: T = 200–300 °C; P = 3.0 MPa; WHSV = 32 h^{-1}.
[a] Tested with a feed containing 20,000 ppm DBF.

When the feed amount is increased to 40,000 ppm DBF) there is a slight decrease in HDO conversion, but it still remains close to 98% after 12 h on stream. As for the product selectivity, BCH was the main product observed in all cases regardless of the amount of DBF feed. The results obtained suggest that nickel phosphide catalysts do not suffer from deactivation under the presence of water formed during the reaction; sintering of the catalysts metal deposition (specifically alkali metals); or coking. It is found that the extent of these phenomena depends strongly on the catalyst employed. Often for HDO reactions carbon deposition is the main cause of catalyst deactivation [48] and the main factor to consider when designing catalysts. It is reported in the literature that coking increases with increasing acidity of the catalyst [49] as Brönsted acid sites are responsible for coke formation. While Lewis acid sites bind species to the catalyst surface, Brönsted sites act as proton donors forming carbocations which are believed to be responsible for coking. Since acid sites are required in the mechanism of HDO, a balance should be achieved in order to have acid sites capable of activate oxygen containing molecules whose strength will not be so strong as to favor coke formation. The carbon deposited on spent Ni_2P-5 catalyst after 12 h of TOS with different DBF concentrations was measured by CNH elemental analysis (Table 4). As reported in this table, the increase of the DBF concentration in the feed results in an increase in the carbon content on the spent catalyst. This mainly occurs when 40,000 ppm of DBT is fed. As no major deactivation is observed, this high carbon content could be ascribed to the retention of some intermediate molecules on the catalyst surface. It is reported that transition metal phosphides are able to form products less susceptible to coke formation [26].

In order to clarify the role of phosphorus, three catalysts with different initial P/Ni molar ratios (1, 2 and 3) and a nickel loading of 5 wt.% were also prepared and their activity tested at 300 °C with a TOS of 12 h. Fig. 6 plots the evolution of conversion for catalysts presenting P/Ni molar ratios of 1, 2 and 3. At 300 °C, all catalysts show high conversions close to 100% during the first 2 h. Thereafter,

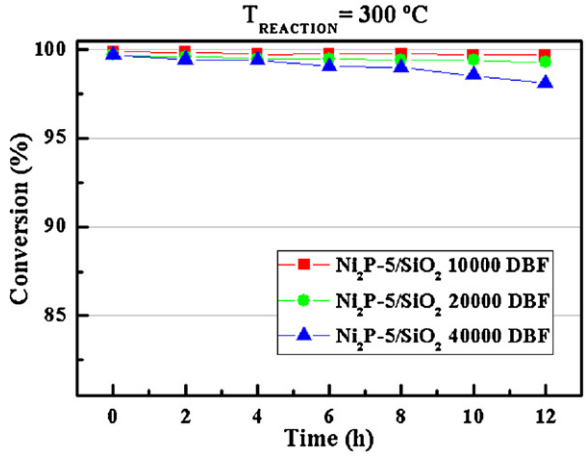

Fig. 5. Evolution of conversion as a function of time on stream for Ni_2P-5 catalyst tested under different amounts of oxygen-containing molecules. Experimental conditions: T = 300 °C; P = 3.0 MPa; WHSV = 32 h^{-1}.

Table 4
Carbon content on spent Ni_2P-5 catalysts after TOS = 12 h obtained from CNH elemental analysis.

Ni_2P-5 catalyst with different feeds		Ni_2P-5 catalysts with different P/Ni initial ratio[a]	
Catalyst	C (%)	Catalyst	C (%)
Ni_2P-5-10,000 ppm DBF	1.8	Ni_2P-5- P/Ni = 1	2.3
Ni_2P-5-20,000 ppm DBF	2.2	Ni_2P-5- P/Ni = 2	2.2
Ni_2P-5-40,000 ppm DBF	5.6	Ni_2P-5- P/Ni = 3	1.7

Experimental conditions: T = 300 °C; P = 3.0 MPa; WHSV = 32 h^{-1}.
[a] Tested with a feed containing 20,000 ppm DBF.

catalysts with an initial P/Ni molar ratio of 2 and 3 do not suffer deactivation for 12 h on stream, displaying high stability. However the catalyst with the lowest initial P/Ni molar ratio undergoes a gradual deactivation during the catalytic test, with also the specific activity being lower for this catalyst (Table 3). The selectivity trend remains unaltered with the P/Ni molar ratio, with BCH being the main product detected for all catalysts. The amount of carbon present in the catalysts containing the different P/Ni molar ratios is very similar and always low (<2.3%), which indicates that deactivation by coke is probably not occurring [50]. Since the Ni_2P-5-P/Ni = 1 sample shows a considerable decrease in conversion while presenting a similar carbon content as the others, it can be deduced that the phosphorus content is playing an important role in preventing deactivation (Table 1). Indeed, examination of the XRD patterns (Fig. 2) show that only the sample Ni_2P-5-P/Ni = 1 has not formed pure Ni_2P, but instead a phosphorus poor $Ni_{12}P_5$ phase. A previous work has shown that $Ni_{12}P_5$ has lower activity and stability than Ni_2P in HDS [29], probably because the $Ni_{12}P_5$ structure is susceptible to attack by H_2S nucleophilic species. The same probably occurs in this case with H_2O as the nucleophile. It is also possible that excess phosphorus in the form of phosphate for the P-rich samples interacts with H_2O, and helps protect the Ni_2P phase.

Thus, the surface composition of spent catalysts with different P/Ni molar ratios was evaluated by XPS. The P 2*p* core level spectra (Fig. 7) reveal that the catalyst with the highest P/Ni molar ratio possesses a greater contribution of signal at 134.3 eV assignable to PO_4^{3-} species compared to the contribution located at *ca.* 133.1 eV assignable to unreduced phosphite species [30]. These data suggest that water interacts with the excess phosphate species present on the catalyst surface thus preventing the oxidation of the nickel phosphide particles. Thus, the catalyst with the lowest amount of phosphorus (P/Ni = 1) is more susceptible to deactivation by water, as indicated in Fig. 6. Previous works [25,51] have explained the great oxidation resistance of Ni_2P phase under water molecules

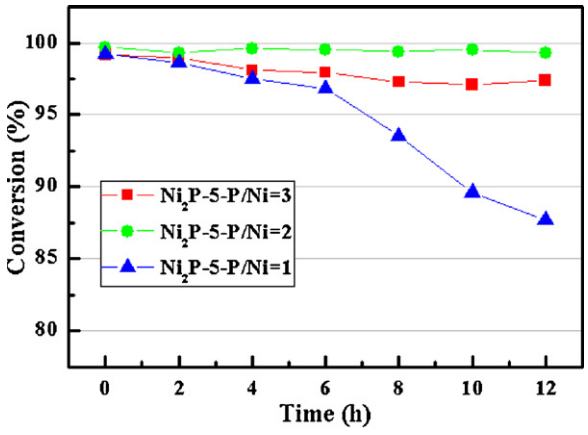

Fig. 6. Evolution of conversion as a function of time on stream for Ni_2P-5 catalysts with different P/Ni initial atomic ratio. Experimental conditions: T = 300 °C; P = 3.0 MPa; WHSV = 32 h^{-1}; Feed: 20,000 ppm of DBF.

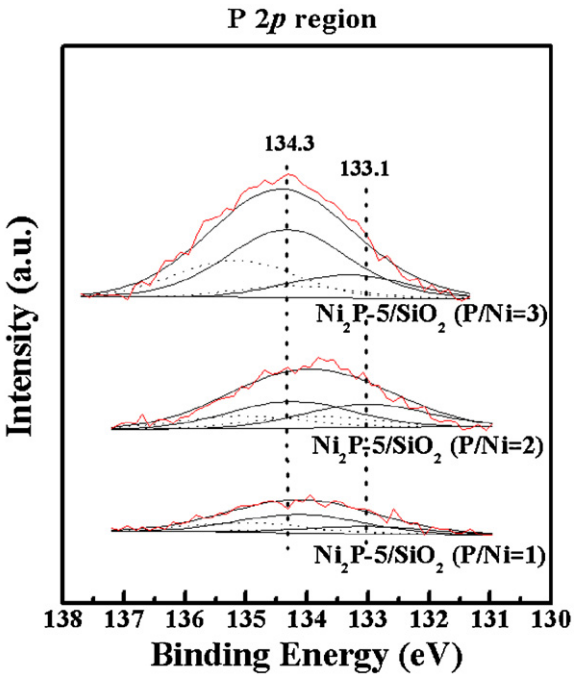

Fig. 7. P 2*p* core level spectra of spent catalysts with different initial P/Ni atomic ratio.

considering that the dissociation of water on Ni_2P (0 0 1) surface gives rise to O atoms interacting with both P and Ni atoms but mainly with P. As a result, oxy-phosphide species are generated with an electron transfer from P to O. Because of a ligand effect of P, the P species may inhibit the combination of Ni with O, enhancing the oxidation resistance of Ni_2P.

The catalyst design for a Ni_2P sample presenting excess P is depicted in Fig. 8. Thus the extra phosphorous on the catalysts surface interacts in a preferential way with water molecules, protecting Ni_2P particles from oxidation and also probably from agglomeration.

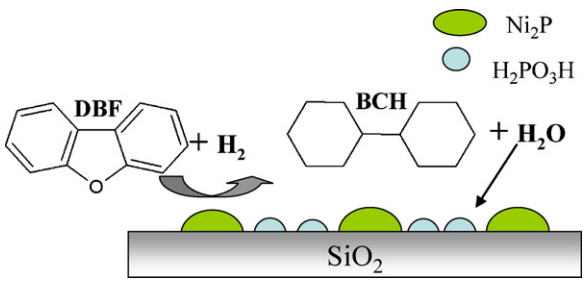

Fig. 8. Proposed Ni_2P catalyst design presenting P excess in the HDO reaction of DBF.

4. Conclusions

Ni_2P catalysts prepared from phosphite type precursors and supported on commercial silica Cab-Sil display very good catalytic properties in the oxygen removal of a bio-oil model compound, benzofuran (DBF). Contact time measurements show that the hydrodeoxygenation sequence over Ni_2P based catalysts involves hydrogenated intermediates.

Benzofuran → Tetrahydrobenzofuran → Hexahydrobenzofuran

→ 2-Phenyl-1-cyclohexanol → Bicyclohexane

Bicyclohexane is the main O-free product observed in all cases (yields > 75% at 300 °C). Catalysts prepared with a low metallic loading (5 wt.%) show a very good catalytic behavior with conversions close to 100% at 300 °C and deoxygenated compounds as the main reaction products observed in all cases, even when feeding very high amounts of oxygenated compound (40,000 ppm DBF).

Nickel phosphide based catalysts show a high resistance to deactivation by coke formation although water produced as a by-product could be the responsible for the slight lowering of conversion. Nonetheless catalysts presented high excess of P did not suffer deactivation under high O-concentration likely due to the preferential interaction of water with the excess phosphorous present on the catalyst surface which protects nickel phosphide particles from oxidation.

Acknowledgments

We gratefully acknowledge support from the Ministry of Science and Innovation, Spain (Ministerio de Ciencia e Innovación, España) through the projects MAT2009-10481, CTQ2012-37925-C03-03 and FEDER funds. A.I.M. thanks the Ministry of Science and Innovation, Spain (Ministerio de Ciencia e Innovación, España) for a Juan de la Cierva contract. STO acknowledges support from the US Department of Energy, Office of Basic Energy Sciences, through Grant DE-FG02-963414669, and the Japan Ministry of Agriculture, Forestry, and Fisheries (Norinsuisansho).

References

[1] G. Yang, E.A. Pidko, E.J.M. Hensen, Journal of Catalysis 295 (2012) 112.
[2] A.V. Bridgwater, Biomass and Bioenergy 38 (2012) 68.
[3] D. Mohan, C.U. Pittman Jr., P.H. Steele, Energy & Fuels 20 (2006) 848–889.
[4] A.V. Bridgwater, Catalysis Today 116 (1996) 285–295.
[5] A. Oasmaa, S. Czernik, Energy & Fuels 13 (1999) 914–921.
[6] S.R.A. Kersten, W.P.M. van Swaaij, L. Lefferts, K. Seshan: G. Centi, R.A. van Santen (Eds.), Catalysis for Renewable-From Feedstocks to Energy Production, Wiley-VCH, Wienheim, 2007 (Chapter 6) p. 119.
[7] E. Furimsky, Applied Catalysis A: General 199 (2000) 147–190.
[8] R.G. Leliveld, S.E. Eijsbouts, Catalysis Today 130 (2008) 183–189.
[9] Y. Romero, F. Richard, Y. Renème, S. Brunet, Applied Catalysis A: General 353 (2009) 46–53.
[10] A.Y. Bunch, U.S. Ozkan, Journal of Catalysis 206 (2002) 177–187.
[11] A.Y. Bunch, W. Wang, U.S. Ozkan, Journal of Molecular Catalysis A: Chemical 270 (2007) 264–272.
[12] E. Laurent, B. Delmon, Applied Catalysis A: General 109 (1994) 97–115.
[13] T.R. Viljava, R.S. Komulainen, T. Selvam, A.O.I. Krause, Studies in Surface Science and Catalysis 127 (1999) 145–152.
[14] O.I. Senol, T.R. Viljava, A.O.I. Krause, Catalysis Today 106 (2005) 186–189.
[15] O.I. Senol, T.R. Viljava, A.O.I. Krause, Applied Catalysis A: General 326 (2007) 236–244.
[16] N. Li, G.W. Huber, Journal of Catalysis 270 (2010) 48–59.
[17] J. Wildschut, F.H. Mahfud, R.H. Venderbosch, H.J. Heeres, Industrial & Engineering Chemistry Research 48 (2009) 10324–10334.
[18] A. Gutierrez, R.K. Kaila, M.L. Honkela, R. Slioor, A.O.I. Krause, Catalysis Today 147 (2009) 239–246.
[19] S. Ramanathan, S.T. Oyama, Journal of Physical Chemistry 99 (1995) 16365–16372.
[20] W. Zhang, Y. Zhang, L. Zhao, W. Wei, Energy & Fuels 24 (2010) 2052–2059.
[21] C. Sepulveda, K. Leiva, R. García, L.R. Radovic, I.T. Ghampson, W.J. DeSisto, J.L.G. Fierro, N. Escalona, Catalysis Today 172 (2011) 232–239.
[22] J. Monnier, H. Sulimma, A. Dalai, G. Caravaggio, Applied Catalysis A: General 382 (2010) 176–180.
[23] W. Wang, Y. Tang, H. Luo, W. Liu, Catalysis Communications 11 (2010) 803–807.
[24] V.M.L. Whiffen, K.J. Smith, Energy & Fuels 24 (2010) 4728–4737.
[25] K. Li, R. Wang, J. Chen, Energy & Fuels 25 (2011) 854–863.
[26] H.Y. Zhao, D. Li, P. Bui, S.T. Oyama, Applied Catalysis A: General 391 (2011) 305–310.
[27] R.H. Bowker, M.C. Smith, M.L. Pease, K.M. Slemkamp, L. Kovarik, M.E. Bussell, ACS Catalysis 1 (2011) 917–922.
[28] S.T. Oyama, Journal of Catalysis 216 (2003) 343–352.
[29] S.T. Oyama, X. Wang, Y.K. Lee, K. Bando, F.G. Requejo, Journal of Catalysis 210 (2002) 207–217.
[30] J.A. Cecilia, A. Infantes-Molina, E. Rodríguez-Castellón, A. Jiménez-López, Journal of Catalysis 263 (2009) 4–15.
[31] J.A. Cecilia, A. Infantes-Molina, E. Rodriguez-Castellon, A. Jimenez-Lopez, Applied Catalysis B: Environmental 92 (2009) 100–113.
[32] J.A. Cecilia, A. Infantes-Molina, E. Rodriguez-Castellon, A. Jimenez-Lopez, Journal of Physical Chemistry C 113 (2009) 17032–17044.
[33] A. Wang, L. Ruan, Y. Teng, X. Li, M. Lu, J. Rena, Y. Wang, Y. Hu, Journal of Catalysis 229 (2005) 314–321.
[34] K.K. Bando, Y. Koike, T. Kawai, G. Tateno, S.T. Oyama, Y. Inada, M. Nomura, K. Asakura, Journal of Physical Chemistry C 115 (2011) 7466–7471.
[35] A. Infantes-Molina, J.A. Cecilia, B. Pawelec, J.L.G. Fierro, E. Rodríguez-Castellón, A. Jiménez-López, Applied Catalysis A: General 390 (2010) 253–263.
[36] A. Rodriguez, J.-Y. Kim, J.C. Hanson, S.J. Sawhill, M.E. Bussell, Journal of Physical Chemistry B 107 (2003) 6276–6285.
[37] T.I. Koranyi, Z. Vít, D.G. Poduval, r. Ryoo, H.S. Kim, E.J.M. Hensen, Journal of Catalysis 253 (2008) 119–131.
[38] S.J. Sawhill, K.A. Layman, D.R. Van Wyk, M.H. Engelhardb, C. Wang, M.E. Bussel, Journal of Catalysis 231 (2005) 300–313.
[39] I.I. Abu, K.J. Smith, Applied Catalysis A: General 328 (2007) 58–67.
[40] K. Lee, S.T. Oyama, Journal of Catalysis 239 (2006) 376–389.
[41] S. Krishnamurthy, S. Panvelker, Y.T. Shah, AIChE Journal 27 (1981) 994–1001.
[42] P.A. Hertan, F.P. Larkins, W.R. Jackson, Fuel Processing & Technology 10 (1985) 121–130.
[43] V. La Vopa, C.N. Satterfield, Energy & Fuels 4 (1987) 323–331.
[44] C. Li, Z. Xu, B.C. Gates, L. Petrakis, Industrial & Engineering Chemistry Process Design and Development 24 (1985) 92–97.
[45] C. Zhao, J. He, A.A. Lemonidou, X. Li, J.A. Lercher, Journal of Catalysis 280 (2011) 8–16.
[46] V.M.L. Whiffen, K.J. Smith, Energy & Fuels 24 (2010) 4728–4737.
[47] T. Uecker, R. Lamber, N.I. Jaeger, U. Schubert, Applied Catalysis A: General 155 (1997) 75–85.
[48] P.M. Mortensen, J.D. Grunwaldt, P.A. Jensen, K.G. Knudsen, A.D. Jensen, Applied Catalysis A: General 407 (2011) 1–19.
[49] E. Furimsky, F.E. Massoth, Catalysis Today 52 (1999) 381–495.
[50] V.N. Bui, D. Laurenti, P. Delichère, C. Geantet, Applied Catalysis B: Environmental 101 (2011) 246–255.
[51] P. Liu, J.A. Rodríguez, Y. Takahashi, K. Nakamura, Journal of Catalysis 262 (2009) 294–303.